FABRICATION AND DOSIMETRIC CHARACTERIZATION OF NOVEL TISSUE-EQUIVALENT *RHIZOPHORA SPP*. PHANTOMS FOR RADIATION THERAPY APPLICATIONS

SAMSON DAMILOLA OLUWAFEMI

UNIVERSITI SAINS MALAYSIA

2021

FABRICATION AND DOSIMETRIC CHARACTERIZATION OF NOVEL TISSUE-EQUIVALENT *RHIZOPHORA SPP*. PHANTOMS FOR RADIATION THERAPY APPLICATIONS

by

SAMSON DAMILOLA OLUWAFEMI

Thesis submitted in fulfilment of the requirements
for the degree of
Doctor of Philosophy

January 2021

ACKNOWLEDGEMENT

I give all my adoration to Almighty God for showering me with His mercies, grace, blessings, protection, support, knowledge, and discipline to complete this work successfully.

I am indebted to my main supervisor, Prof. Dr. Mohd Zubir Bin Mat Jafri, for the substantial guidance, advice, support, wisdom, and kindness. He was always available, never get tired of my interruption, and generously shared his valuable time, I will forever be thankful to him. I am also grateful to my co-supervisor and mentor, Prof. Dato' Dr. Ahmad Shukri Bin Mustapa Kamal, for the invaluable discussions and opinions that would never have begun, let alone completed this work without him. He shared his experience with me, with respect and enthusiasm. I am so grateful for his continuing guidance, support, motivation, and help in making sure that I get the supplies I needed on time, even though it is not convenient for him.

For my second co-supervisor Prof. Dr. Rokiah Binti Hashim, I express my sincere gratitude for having invaluable insights into the fundamentals of particleboard. She far surpassed my expectations and provide me with useful suggestions and support. My highest appreciation also goes to my third co-supervisor Dr. Mohd Zahri Bin Abdul Aziz for sharing his experience with me for most of my work with great patience, useful guidance, and perspective.

My sincere appreciation to all staff of the School of Physics, Universiti Sains Malaysia, Malaysia, for their guidance, support, and encouragement. I have gained a lot of scientific knowledge from you all and I will always remember and be thankful for your contributions in this research. My gratitude also extended to Dr. Mohd Fahmi

Mohd Yusof for his advice and suggestions on the sample characterization from the start of this study until the end. I am most grateful to Mr. Basrul, Mr. Azhar, Mr. Rizal, Mr. Azahari, and Mrs. Kak Fizah for their regular assistant in the sample preparation and analysis.

My greatest appreciation to the Universiti Sains Malaysia, Malaysia, for having awarded me the Graduate Assistant Scheme for one year and the Fundamental Research Grant Scheme (203/PTEKIND/6711525 and 304/PFIZIK/6316173) during this research.

My deep appreciation also goes to the Vice-Chancellor and Management of the University of Abuja, Nigeria, for providing a fund through the Tertiary Education Trust Fund (TETF) (NEEDS Assessment)/Academic Staff Training and Development (AST&D) scholarship during the time of this work. I am also very thankful to all the staff in the Department of Physics, University of Abuja for all their support and encouragement.

My overwhelming thanks go to my mother, my siblings, my in-laws for their prayers, guidance, encouraging words, financial and moral support.

My love and appreciation go to my adorable wife and son, you are my hero. I am grateful for the trust you have in me, and for helping me get this far. Thank you in my absence for all the sacrifices you have rendered for running the home front. To me, it means the whole world.

Finally, to my late Dad, thank you for growing me up to the very best. You provide support for a lifetime and you gave me the resources to develop my professional life and taught me the fundamental moral principles to face life. I dedicated this thesis to you.

TABLE OF CONTENTS

LIST OF TABLES

Page

LIST OF FIGURES

Page

LIST OF SYMBOLS

°C	Degree Celsius
^{137}Cs	Cesium-137
^{60}Co	Cobalt-60
d_{max}	Depth at maximum dose
d_{ref}	Depth at reference dose
I_o	Beam intensity at a reference point
I_t	Transmitted beam intensity
λ	Wavelength
ρ	Density
μ	Linear attenuation coefficient
μ_m	Mass attenuation coefficient
$\mu_{(x,y)}$	Photon linear attenuation coefficient for DSF-SPC-SPI-*R. spp.*
μ_{water}	Photon linear attenuation coefficient of water
$X_{1/2}$	Half-value layer
Z_{eff}	Effective atomic number

LIST OF ABBREVIATIONS

AAPM	American Association of Physicists in Medicine
AE	Lowest energy for electrons
AIDR	Adaptive iterative dose reduction
ANOVA	Analysis of variance
AP	Lowest energy for photons
CT	Computed tomography
C_rI	Crystallinity index
CIRS	Computerized imaging reference system
DSF	Defatted soy flour
DSC	Differential scanning calorimetry
DETA	Diethylenetriamine
DTG	Derivative thermogravimetric
ECH	Epichlorohydrin
EDP	Electron density phantom
EDXA	Energy dispersive X-ray spectroscopy analysis
EGSnrc	Electron Gamma Shower by National Research Council
ECUT	Electron transport cut-off energy
EBT	Extended beam therapy
EBRT	External beam radiation therapy
FE-SEM	Field emission scanning electron microscopy
FT-IR	Fourier transform infrared
FWHM	Full width half maximum
GEANT	Geometry and tracking
GeV	Giga-electron volt
^{1}H-NMR	Proton nuclear magnetic resonance
HU	Hounsfield Units
IA-PAE	Itaconic acid polyamidoamine-epichlorohydrin
IAEA	International Atomic Energy Agency
IB	Internal bonding
IC	Ionization chamber
ICRU	International Commission on Radiation Units and Measurements

IGRT	Image-guided radiation therapy
IMRT	Intensity-modulated radiation therapy
JIS	Japanese industrial standards
keV	Kilo-electron volt
kVp	Kilo-voltage peak
LINAC	Linear accelerator
LEGe	Low energy germanium
MC	Monte Carlo
MCNP	Monte Carlo neutron-particle
MCA	Multichannel analyzer
MFP	Mean free path
MLC	Multileaf collimator
MOR	Modulus of rupture
MOE	Modulus of elasticity
MOSFET	Metal-oxide semiconducting field-effect transistor
MeV	Mega-electron volt
MRI	Magnetic resonance imaging
MU	Monitor Unit
MUF	Melamine-urea-formaldehyde
MV	Megavolt
NaOH	Sodium hydroxide
OD	Optical density
OAR	Off-axis ratio
OSL	Optically-stimulated luminescence
PDD	Percentage depth dose
PCUT	Photon transport cut-off energy
PEGS4	Pre-electron gamma shower 4
PENELOPE	Penetration and energy loss of positrons and electrons
PET	Positron emission tomography
PF	Phenol-formaldehyde
pH	Potential of hydrogen
QA	Quality assurance
QC	Quality control
RAP	Radiation attenuation parameters

RED	Relative electron density
RF	Radiofrequency
ROI	Region-of-interest
RT	Radiation therapy
RTD	Radiation therapy dosimetry
R. spp.	*Rhizophora spp*.
SBRT	Stereotactic body radiation therapy
SC	Solid content
SPC	Soy protein concentrate
SPI	Soy protein isolate
SPSS	Statistical package for social sciences
SRS	Stereotactic radiosurgery
SSD	Source-to-surface distance
TEM	Tissue-equivalent material
TEP	Tissue-equivalent phantom
TGA	Thermogravimetric analysis
TEPM	Tissue-equivalent phantom material
TLD	Thermoluminescent dosimeter
TPS	Treatment planning system
$TPR_{20,10}$	Tissue-phantom ratio at depths of 20 cm and 10 cm
TS	Thickness swelling
UF	Urea-formaldehyde
VMAT	Volumetric modulated arc therapy
WA	Water absorption
WEPM	Water-equivalent phantom material
XCOM	X-ray computed
XRD	X-ray diffraction
XRF	X-ray fluorescence

LIST OF APPENDICES

FABRIKASI DAN PENCIRIAN DOSIMETRI FANTOM *RHIZOPHORA SPP.* NOVEL SETARA TISU UNTUK PENGGUNAAN TERAPI SINARAN

ABSTRAK

Fantom yang dibina dari bahan setara tisu (TEM) digunakan untuk menilai dos sinaran yang disampaikan kepada pesakit dan menilai kualiti sistem pengimejan radiologi. Walau bagaimanapun, sangat sedikit daripada bahan ini telah dibangunkan untuk penganggaran dos dengan foton tenaga rendah dan tinggi dan elektron tenaga tinggi menggunakan papan zarah *Rhizophora spp*. (*R. spp*.) dengan perekat berasaskan bio. Reka bentuk, fabrikasi dan ciri-ciri papan zarah sebagai bahan fantom setara tisu (TEPM) baharu dengan sifat dosimetri yang sesuai pada tenaga foton diagnostik dan terapi serta tenaga elektron terapi dijelaskan. Kepentingan TEM yang dibangunkan dalam kajian ini adalah untuk menyumbang kepada pembinaan fantom papan zarah berkualiti tinggi dalam aspek klinikal dan penyelidikan dosimetri terapi sinaran. Fantom papan zarah *R. spp*. dibangunkan dengan memasukkan tepung soya nyahlemak (DSF), protein soya pekat (SPC), protein soya terasing (SPI), zarah *R. spp*. pada tiga saiz berbeza (149–500, 74–149, dan ≤ 74 μm), natrium hidroksida (10% berat), dan empat tahap rawatan asid itakonik polyamidoamine-epichlorohydrin (IA-PAE) yang berbeza (0, 5, 10, dan 15% berat). Parameter pengecilan sinaran (RAP) ditentukan menggunakan pancaran pendarfluor sinar-X dalam julat 16.59–25.26 keV dan foton dari ^{137}Cs dan ^{60}Co. Fantom ini kemudian diimbas menggunakan tomografi berkomputer (CT) dengan voltan tiub sinar-X 80, 120, dan 135 kVp. Ciri-ciri dosimetri diuji menggunakan kebuk pengionan dan dosimeter filem Gafchromic EBT3 untuk foton 6 dan 10 MV dan elektron 6, 9, 12, dan 15 MeV. Sampel fantom dengan penambahan IA-PAE hingga 15% berat dan saiz zarah ≤ 74 μm yang mempamerkan

kualiti optimum didapati sebanding dengan air (program WinXCom) dengan nilai $p > 0.05$. Kebarangkalian interaksi foton yang dikira dengan kod Monte Carlo EGSnrc PEGS4 mendedahkan ketekalan fantom *R. spp*. dengan fantom air dan fantom air pepejal. Nilai $TPR_{20,10}$ yang dikira menunjukkan bahawa peratus perbezaan adalah 0.29–0.72%, 0.58–1.00%, dan 0.29–0.72% untuk foton 6 MV. Begitu juga, perbezaan untuk foton 10 MV berada dalam julat yang boleh diterima 0.26–0.65%, 0.52–0.91%, dan 0.52–0.91%. Juga, didapati bahawa perbezaan relatif dalam d_{max} dengan fantom air dan fantom air pepejal dalam kalangan sampel fantom *R. spp*. berada dalam julat 1.08–2.96% untuk foton 6 MV, sementara untuk foton 10 MV adalah 7.42–10.03%. Tidak terdapat perbezaan yang signifikan untuk profil alur pada d_{ref} dan d_{max} dengan fantom air pepejal. Ini menunjukkan kehomogenan dos yang baik. Perbezaan dalam lengkung PDD menggunakan elektron 6, 9, 12, dan 15 MeV dengan fantom air dan air pepejal berada dalam lingkungan 4.40–6.84%. Perbandingan antara parameter dosimetri yang diukur menggunakan filem Gafchromic EBT3 pada semua kedalaman menunjukkan ketekalan yang baik dengan perbezaan dalam linkungan 2% dan 9% untuk foton 6 dan 10 MV. Hasil sama diperolehi dengan perbezaan dalam julat yang boleh diterima dari 2.0–6.5% untuk elektron 6, 9, 12, dan 15 MeV masing-masing. Penemuan ini menunjukkan bahawa perbezaan antara fantom papan zarah *R. spp.* berasaskan DSF-, SPC-, dan SPI berbanding fantom air dan air pepejal adalah tidak signifikan. Hasil tersebut telah mengesahkan kesesuaian fantom papan zarah *R. spp.* berasaskan DSF-, SPC-, dan SPI-NaOH/IA-PAE dengan perekat 15% berat IA-PAE dan ukuran zarah $\leq$ 74 μm sebagai TEPM dosimetri yang sesuai untuk penggunaan terapi sinaran.

FABRICATION AND DOSIMETRIC CHARACTERIZATION OF NOVEL TISSUE-EQUIVALENT *RHIZOPHORA SPP*. PHANTOMS FOR RADIATION THERAPY APPLICATIONS

ABSTRACT

Phantoms constructed from tissue-equivalent materials (TEMs) are used to assess radiation dose delivered to patients and evaluate the quality of radiological imaging systems. However, very few of these materials have been developed for dose estimations with low and high energy photon and high energy electron beams using *Rhizophora spp.* (*R. spp*.) particleboards with a bio-based adhesive. The design, fabrication and properties of *R. spp*. particleboards as novel tissue-equivalent phantom material (TEPM) with suitable dosimetric properties at diagnostic and therapeutic photon and therapeutic electron energies are described. The importance of TEMs developed in this study is to contribute to the construction of high-quality particleboard phantoms in both clinical and investigative aspects of radiation therapy dosimetry. The *R. spp.* particleboard phantoms were developed by incorporating defatted soy flour (DSF), soy protein concentrate (SPC), soy protein isolate (SPI), *R. spp.* particles at three different sizes (149–500, 74–149, and ≤ 74 μm), sodium hydroxide (10 wt%), and four different treatment levels of itaconic acid polyamidoamine-epichlorohydrin (IA-PAE) (0, 5, 10, and 15 wt%). Radiation attenuation parameters (RAPs) were ascertained using X-ray fluorescence emissions ranging from 16.59–25.26 keV and photons from ^{137}Cs and ^{60}Co. These phantoms were further scanned using computed tomography (CT) with X-ray tube voltages of 80, 120, and 135 kVp. The dosimetric characteristics were tested using an ionization chamber and Gafchromic EBT3 film dosimeters for 6 and 10 MV photons and 6, 9, 12, and 15 MeV electrons. Phantom

samples with up to 15 wt% of IA-PAE addition and particle size of ≤ 74 μm which demonstrated optimum qualities were found to be comparable with that of water (WinXCom program) with p-values > 0.05. The probability of photon interactions calculated with the Monte Carlo code EGSnrc PEGS4 revealed the consistency of *R. spp*. phantoms with water and solid water phantoms. The calculated $TPR_{20,10}$ values indicates that percentage discrepancies were 0.29–0.72%, 0.58–1.00%, and 0.29–0.72% for 6 MV photons. Likewise, the discrepancies for 10 MV photons were within the acceptable range of 0.26–0.65%, 0.52–0.91%, and 0.52–0.91%. Also, it was found that the relative difference in the d_{max} to water and solid water phantoms among the *R. spp*. phantom samples were within the range of 1.08–2.96% for 6 MV photons, while those of 10 MV photons were 7.42–10.03%. No significant difference was found for beam profiles at d_{ref} and d_{max} with solid water phantoms, demonstrating good dose homogeneity. The discrepancies between the PDD curves with 6, 9, 12, and 15 MeV electrons with those of water and solid water phantoms were in the range of 4.40–6.84%. Comparison between the measured dosimetric parameters using Gafchromic EBT3 films at all depths indicates good consistency with a difference within 2% and 9% for 6 and 10 MV photons. Comparable results were found with discrepancies within an acceptable range of 2.0–6.5% for 6, 9, 12, and 15 MeV electrons, respectively. These findings revealed that the discrepancies between DSF-, SPC-, and SPI-based *R. spp*. particleboard phantoms with that of water and solid water phantoms were insignificant. The results have quantified the appropriateness of DSF-, SPC-, and SPI-NaOH/IA-PAE-based *R. spp*. particleboard phantoms with 15 wt% IA-PAE adhesive and particle size of ≤ 74 μm as suitable dosimetric TEPM for radiation therapy applications.

CHAPTER 1

INTRODUCTION

1.1 Background of the Study

Radiation dosimetry has its provenance in the medical application of ionizing radiation following the discovery of X-rays by Wilhelm Röentgen (1895), radioactivity by Henri Becquerel (1896), and radium from uranium ore by Pierre and Marie Curie (1898) (Kienbock, 1906). Shortly after that, Robert Abbe of New York utilized radium for medical therapy, and Howard Kelly of Baltimore pioneered radium treatment of cervical cancer. Since then radiation therapy (RT) has developed into a significant modality for the treatment of many cancers. Almost every known consequence of ionizing radiation on matter, whether physical, chemical or biological, has been suggested as a foundation for radiation dosimetry, particularly if the material can be made dosimetrically tissue-equivalent (Khan, 2010; Eaton, 2015).

RT can be described as the medical use of ionizing radiation during cancer treatment to control malignant cells, and is usually paired with surgery and/or chemotherapy. It focuses on optimizing the effective dose given to the treatment volume while reducing the dose to the healthy tissue or organs surrounding it. Generally, RT is classified into two major categories: teletherapy (external beam RT) and brachytherapy (internal RT) (Zabihzadeh et al., 2013). In teletherapy, the source of radiation is typically at a certain distance from the patient, and the radiation beam irradiates the target within the patient. As for brachytherapy, miniature radioactive isotopes are inserted directly into the target volume (intracavitary or interstitial brachytherapy) or onto a target (intraoperative RT) (DeWerd, 2014).

As new strategies for delivering radiation to patients become increasingly complex and innovative, great interest has been created in various forms of conformal treatment planning and calculations that integrate small field dosimetry such as intensity-modulated radiation therapy (IMRT), stereotactic radiosurgery (SRS), and stereotactic body radiation therapy (SBRT) (Bustillo et al., 2018). IMRT involves the delivery of optimized, non-uniform irradiation beam intensities. A uniform dose distribution can be generated around the tumor by modulating the intensity of the beam from a linear accelerator (LINAC) (Okkalidis et al., 2018).

The LINAC is a device that uses high frequency electromagnetic waves to accelerate charged particles, such as electrons, to high energies through a linear tube. The device also includes multiple standardized safety mechanisms to ensure the exact dose as indicated in the treatment planning system (TPS). The effectiveness of the planned dose from the TPS and its effect depends entirely on the delivered dose at the patient's respective site with reproducible accuracy or within tolerance of the planned dose. There are several techniques available to equate the dose administered with the expected dose. In general, absolute dosimetry is preferred using an ionization chamber with which point dose is measured at the specified and reference depth (Fraser et al., 2009).

In the case of reference dosimetry, quality assurance (QA) is performed in which radiochromic film is placed in the slab phantom at a given depth at which the dose distribution is to be measured. The expected dose is then delivered and the resulting density of the film can be correlated with dose at each point on the film, which can be compared with the planned dose distribution. There are different techniques for achieving accuracy in dosimetry, and they are based on guidelines of

the International Atomic Energy Agency (IAEA) recommendations published in technical reports series numbers 277 and 398 (IAEA, 1997; 2000).

Phantoms are essentially surrogates for human tissue and have become critical tools for a variety of radiation dose measurement applications. They have become essential for QA and quality control (QC) in a variety of medical procedures involving radiation. Acceptable phantom material for radiation dosimetry must resemble the human body and anatomy, and in terms of its radiation parameters, it must be made with materials that are proportionate to human soft tissues herein called tissue-equivalent materials (TEM) or tissue substitute materials. TEM is characterized as the materials that substitute original human tissue and organs for a given radiation form and energy by absorbing and scattering the radiation within known and reasonable limits to the same extent as actual tissues (ICRU, 1992).

Water is one of the significant reference phantom materials used in medical radiation centers for QA because of its particular radiation attenuation characteristics (DeWerd, 2014). Nevertheless, due to its liquidity and the fact that some radiation dosimetric tools are not suitable for use in water, its use is not always practical (Khan, 2010). It has been one of the more challenging endeavours in the field of tissue simulation to precisely mimic water for photons and electrons over a wide range of energies using a specific solid material. When water is utilized, the water container is vulnerable to mechanical instability and if it is of a sealed form, there can be a problem of maintaining the purity of the water. Tissue-equivalent phantoms (TEPs) are estimable to experimental biomedical research given that they could provide a better simulation of real human tissue, as well as aid in the development and validation of the modalities in medical applications (Wang et al., 2016).

The choice of these suitable tissue-equivalent phantom materials (TEPMs) is crucial to the pattern and function of any form of the phantom. Thus, different solid homogenous water-equivalent phantom materials (WEPMs) have been produced in different shapes with various materials and are extensively used currently as phantom for QA and radiation dosimetry to replace water (Khan, 2010; DeWerd, 2014). However, due to variations of their densities and dissimilarities of elemental compositions, the use of these WEPMs lacks the capability to produce good simulation to water and soft tissues. There has also been continued interest to consider phantoms manufactured using local, renewable, accessible, cheap, biodegradable, biocompatible, and environmental friendly materials such as tropical wood (Bradley et al., 1991; Banjade et al., 2001).

Rhizophora spp. (*R. spp*.) wood, is obtained from an ancient and widely distributed mangrove tree genera that is abundantly grown at the interface between land and sea in tropical and subtropical zones, where they occur in conditions of high salinity, anaerobic soils, extreme tides, strong winds, high temperatures, and muddy waters. Categorically, *R. spp*. could be used as a phantom in two general forms, such as solid raw wood and particleboards.

R. spp. wood in the form of particleboards has been considered as potential phantom material due to their favorable characteristics including homogeneity, malleability, and the fact that they can be fabricated using different particle sizes and shapes, characterizing its similarity in terms of dosimetric properties to water and other typical phantom materials (Shakhreet et al., 2013; Ababneh et al., 2016, Abuarra et al., 2014). Therefore, they make highly attractive materials for accurate tissue substitution for a variety of applications including high energy photon and electron RT as well as X-ray imaging: including low energy breast imaging, computed tomography (CT),

positron emission tomography (PET), magnetic resonance imaging (MRI), nuclear imaging, and many other medical applications (Alshipli et al., 2018; Anugrah et al., 2020).

Raw *R. spp*. wood has the potential to be warped, cracked, degraded, and damaged with time and the diameter of *R. spp*. tree trunks are typically less than 30 cm, which makes them unsuitable to be cut as standard phantoms with the size of 30 × 30 × 30 cm^3 (Marashdeh et al., 2012). On the other hand, the quality of manufactured *R. spp*. particleboards as phantom materials are of great concern because of the overwhelming workload and inflexibility of QA and dosimetry applications in diagnostic radiology and RT (Rabaiee, 2018). Thus, the use of appropriate binders or adhesives with specific characteristics in the fabrication of *R. spp*. particleboards have become a prevailing alternative for improved physical and mechanical properties, and dimensional stability changes with environmental variations, as well as retaining its radiation attenuation parameters (RAPs) and water commensurate properties.

An adhesive denotes a material that can be used to bind two similar or dissimilar surfaces together, thereby forming a bond that is difficult to pull apart if there is no greater force. Over the years, adhesive wood bonding has been the key factor in the successful application of the raw material in the wood industry (Ebnesajjad, 2011). These adhesives can be classified into two major groups: non-renewable resources or synthetic (petroleum)-based and renewable resources or bio-based adhesives.

The non-renewable resources such as formaldehyde-based adhesives, glyoxal, polyvinyl alcohol, and epoxy compounds are the most widely used binders in the wood panel industry (Rokiah et al., 2009). These fossil-based adhesives are fast curing

adhesives that can be transformed fairly easily into well-defined, homogeneous and specifically formulated polymers. They provide good heat, moisture and decay resistance and have dominated the wood product market for structural and exterior wood products (Kim, 2010). Unfortunately, they emit detectable amounts of formaldehyde and other volatile organic compounds (Roffael, 2010), considered to have a narcotic effect on the central nervous system and a local irritation on the mucous membrane. In addition, these materials also failed to retain the physical, mechanical, dimensional stability, and radiation attenuation properties of natural wood composites in comparison to water (Ngu et al., 2015).

Therefore, substantial efforts have been put forth to reduce some problems related to these adhesives for developing inexpensive, economically competitive, biodegradable, biocompatible, and readily available particleboards from renewable resources, thereby reducing cost, increase output, optimize adhesive content, and control formaldehyde emissions. Renewable resources in wood resin manufacture have been validated through specific independent studies, and have been utilized in the formulation of different wood composite adhesive systems by many researchers (Gui et al., 2013; Yusof et al., 2017; Zhang et al., 2017; Ababneh et al., 2016; Shankar et al., 2013; Sara et al., 2010). In fact, soy protein-based adhesives have already been widely regarded as an alternative bio-based wood adhesive in industrial applications (Gui et al., 2013; Pizzi, 2006; He, 2017).

Soy proteins include defatted soy flour (DSF), soy protein concentrate (SPC), and soy protein isolate (SPI). These materials have been globally applied for drug delivery, tissue regeneration, as filtration membranes, and in coating and packaging (Gupta and Nayak, 2015). They are highly oxygenated carbon compounds and this makes them ideal for use in the manufacture of phantom materials equivalent to tissue

and water, and can be used either as adhesive with curing (addition of cross-linking agents) or without curing (Gui et al., 2013; Zhang et al., 2017; Rabaiee, 2018). However, to break the internal bonds and disperse the polar protein molecules a chemical change is necessary (Kumar et al., 2004). To enhance these effects, a significant amount of research has been conducted to modify the molecular structure or conformation of soy proteins through denaturation agents, chemical cross-linking, enzymatic hydrolysis treatments, processing method improvements, organic or inorganic blending, and block co-polymerization (Luo et al., 2016; Li et al., 2016; Obokata and Isogai, 2004; Liu et al., 2017; Gui et al., 2013; Huang et al., 2012; Xia et al., 2015; Zhang et al., 2017).

Owing to its effectiveness, chemical cross-linking reactions among functional groups of soy protein have been confirmed to be one of the most useful techniques in biochemical applications, greatly enhancing the adhesion performance, in particular the wet adhesion strength, by forming an entangled protein complex upon curing (Xia et al., 2015). The chemical cross-linking of sodium hydroxide (NaOH)/itaconic acid polyamidoamine-epichlorohydrin (IA-PAE) curing soy protein-based adhesives has been validated to make wood composite products that meet the standards for particleboards, plywood, and engineered wood flooring, with significant reduction in the dimensional stability, greater enhancement of the physical and mechanical properties and improvement of the thermal stability of the particleboard samples (Gui et al., 2013; Gao et al., 2019).

Introducing a suitable tissue- and water-equivalent phantom material for diagnostic radiology and RT through the modification of a material derived from bio-based resources is of major importance to the future of this medical field. Thus, in this present research, *R. spp*. particleboard phantoms were developed using three *R. spp.*

particle sizes (149–500, 74–149, and ≤ 74 μm) with four IA-PAE adhesive treatment levels (0, 5, 10, and 15 wt%) based on DSF, SPC, SPI, and NaOH (10 wt%). The fabricated particleboards were subjected to in-depth characterizations in order to understand the interfacial mechanism between soy proteins and IA-PAE resin, as well as retaining the radiation attenuation and water commensurate properties of the particleboard phantoms. The performance of the fabricated particleboard phantoms was measured according to the Japanese Industrial Standards (JIS A 5908:2015) procedure and specifications. The RAPs were ascertained using X-ray fluorescence (XRF) emissions at photon energies ranging from 16.59–25.26 keV and photons from ^{137}Cs and ^{60}Co utilising a Ludlum setup. These phantoms were further scanned using X-ray computed tomography (CT) with tube voltages of 80, 120, and 135 kVp. The dosimetric characteristics were tested using an ionization chamber (IC) and Gafchromic EBT3 film dosimeters for 6 and 10 MV photons and 6, 9, 12, and 15 MeV electrons. The manufactured particleboard phantoms were further validated using the Monte Carlo code EGSnrc PEGS4 in the energy range of 0.001–70.0 MeV. The findings were compared with those of appropriate standard phantom materials (water and solid water) in RT.

1.2 Statement of the Research Problem

The use of water as the reference phantom material is due to the fact that, in most cases, it is the preferred medium for dose calculations, from previous clinical experience, and that it acts radiologically in almost exactly the same manner as soft tissue, which consists of 75–90% water (Andreo, 2000). Although, this does seem reasonable, however, there is no statistical proof or adequate scientific evidence that a water phantom can be regarded as equivalent to human tissue. There are difficulties in

maintaining the temperature and humidity of the water phantom and its surroundings. On the other hand, very few of the solid water phantom materials have been constructed and developed in the low and high photon and high electron energies encountered in diagnostic radiology and RT. This is as a result of their being overpriced and hard to obtain, especially in countries going through development.

As an alternative, in diagnostic radiology and RT, particleboard phantoms made from *R. spp*. have been evaluated for radiation dosimetry (Abuarra et al., 2014; Yusof et al., 2017; Alshipli et al., 2018; Anugrah et al., 2020; Zuber et al., 2020). However, many of the phantom materials made of *R. spp*. still failed to produce good simulation to water at various energies (Shakhreet et al., 2013). Furthermore, certain important criteria prevail in the manufacture of such phantom materials, such as the physical dimensions should be reproducible in order to allow for precise dosimetric measurements. In RT applications, more accurate dosimetry treatment deliveries require phantom materials appropriate for high energy photons and electrons. Therefore, phantom materials through the curing of materials obtained from bio-based resources that have the proportionate characteristics of suitable tissue- and water-equivalent phantoms for high energy photons and electrons in RT applications is of major importance.

None of the earlier studies have so far attempted to optimize the properties of *R. spp*. particleboards manufactured using DSF-, SPC-, and SPI-NaOH/IA-PAE adhesives as suitable solid TEPM used for dosimetry work in RT. This current research, therefore, introduces and develops novel solid water tissue substitute *R. spp*. particleboard phantoms based on different rates of IA-PAE and DSF-, SPC-, and SPI-NaOH adhesives to be used for radiation dosimetry of high energy photons and electrons. This phantom has the potential to allow the adjustment of the position of

measurement and dosimeter conveniently, although in this work it is primarily designed for ICs and Gafchromic EBT3 film dosimeters.

1.3 Novelty and Significance of the Study

The significance of this current study is the development and dosimetric characterization of novel solid TEPs made from *R. spp*. particleboards using DSF-, SPC-, and SPI-based adhesives modified with NaOH and IA-PAE for high energy photons and electrons in RT applications. The importance of TEMs developed in this work is to contribute to the construction of high-quality particleboard phantoms with comparable dosimetric characteristics to water and solid water phantoms, and avoid the detectable amounts of formaldehyde emissions and other volatile organic compounds using realistic, durable, and inexpensive bio-based materials. This phantom formulation will be useful in dosimetry of brachytherapy sources, CT, X-ray imaging, and all RT applications up to 10 MV for photons and 15 MeV for electrons. This research points to the possibility of using DSF-, SPC-, and SPI-NaOH/IA-PAE and mangrove wood as potential TEMs for use as phantoms in both clinical and investigative aspects of radiation therapy dosimetry (RTD).

1.4 Aim and Objectives of the Research

The aim of this research is towards the synthesis, development, and dosimetric characterization of novel tissue-equivalent *R. spp*. particleboard phantoms cured with bio-based adhesives for high energy photons and electrons for RT applications.

The research objectives set out in this thesis are listed as follows:

I. To synthesize and investigate the effect of NaOH on DSF-, SPC-, and SPI-based adhesives with different concentrations of the cross-linking agent IA-PAE in order to understand the interfacial mechanism between the adhesives.

II. To develop, characterize and evaluate the physical, mechanical, and dimensional stability properties, effective atomic numbers, RAPs, HU values, RED, and density distribution profiles of DSF-, SPC-, and SPI-NaOH/IA-PAE-based *R. spp*. particleboard phantoms as a new type of TEPM for low and high energy photons and high energy electrons.

III. To evaluate the overall effectiveness of using ICs and Gafchromic EBT3 radiochromic films for dosimetry measurements.

IV. To determine the dosimetric characteristics of the particleboard phantoms and compare them with acceptable standard phantoms for high energy photon (6 and 10 MV) and electron (6, 9, 12, and 15 MeV) beams.

1.5 Scope of the Study

The synthesized IA-PAE was used with NaOH as the resin in the modification of DSF-, SPC-, and SPI-based *R. spp*. particleboard phantoms. The fabricated particleboard phantoms were characterized using ^{1}H-Nuclear magnetic resonance (^{1}H-NMR), differential scanning calorimetry (DSC), thermogravimetry (TG), Fourier transform infrared spectroscopy (FT-IR), field emission scanning electron microscopy (FE-SEM), energy dispersive X-ray spectroscopy (EDX), and X-ray diffraction (XRD) to determine the chemical response, physical properties, thermal stability, thermal degradation, functionalities and types of functional groups, surface morphologies, elemental composition, and structural properties. Three particle size (149–500, 74–

149, and ≤ 74 μm) of *R. spp*. were employed for each of the DSF-, SPC-, and SPI-based bio-adhesives with different concentrations of IA-PAE (0, 5, 10, and 15 wt%) and NaOH (10 wt%).

Moreover, the physical, mechanical, and dimensional stability properties of the binderless, unmodified, and modified particleboard samples were measured and compared according to JIS A 5908:2015. XRF photons were employed in this study and the RAPs were evaluated at 16.59, 17.46, 21.21, and 25.26 keV photon energies. The dose-rate distribution around ^{137}Cs and ^{60}Co radioisotope sources were also determined. The CT numbers, relative electron density (RED), and density distribution profiles were determined at X-ray CT tube voltages of 80, 120, and 135 kVp. Dosimetric properties in comparison to water and solid water phantoms using ICs and Gafchromic EBT3 radiochromic films were performed for high energy photons (6 and 10 MV) and electrons (6, 9, 12, and 15 MeV) to ascertain the tissue-phantom ratio ($TPR_{20,10}$), output calibration, percentage depth doses (PDDs), and beam profiles. The Monte Carlo code EGSnrc PEGS4 was employed to study the histories of photon interactions in the DSF-, SPC-, and SPI-NaOH/IA-PAE bonded *R. spp*. particleboard phantoms and compare the obtained results with those of water and solid water phantoms as the standard phantom materials for RT purposes.

1.6 Thesis Organization

This thesis includes five research chapters. Chapter 1 is the introductory part of the work which discusses the essentials, radiation dosimetry, different forms of RT, and the critical role of phantom materials in RTD, QA, and TPS. Also, the problem statement, novelty and significance of the study, aim and objectives of the research, scope of the study, and thesis organization are discussed in detail.

Chapter 2 provides the RT overview, description of LINAC and its component systems, comparisons of dosimeters in RT, and Monte Carlo simulation using EGSnrc PEGS4. This is followed by a description of the theoretical background of radiation dosimetry for low and high energy photon and high energy electron beams, and the interaction of radiation fields with matter. Overview of adhesives, and effect of NaOH/IA-PAE resin on soy protein matrix are also outlined in this chapter. The last section of this chapter describes dosimetry phantoms and the contributions of other researchers in the areas of fabrication and testing of *R. spp*. particleboard phantoms as TEMs.

Chapter 3 outlines the theoretical considerations, calibration procedures, materials, and various experimental equipment, which were used in this research, such as ^{1}H-NMR, DSC, TGA, FT-IR, FE-SEM, EDXA, XRD, XRF, Ludlum setup, X-ray CT CIRS Model 062M scanner, and WinXcom program. In addition, the synthesis of the adhesives, development, and characterization of the particleboard phantoms, testing of physical, mechanical and dimensional stability properties, RAP measurements, dosimetric characterization of the phantom using ICs and Gafchromic EBT3 radiochromic films in water and solid water phantoms for high energy photon and electron beams are also described. This chapter further reports the probability of photon interactions and a comparison of the measured results with Monte Carlo EGSnrc PEGS4 simulations.

Chapter 4 concentrates on the results and discussions of all experiments carried out in this study: the synthesis, characterization of physical and mechanical properties, dimensional stability, RAPs, PDD, tissue-phantom ratio, beam profiles as well as dose estimation for all the three types of soy protein-based phantom materials which are compared with those of water and solid water phantoms. The variations in the

fractional interaction probability of photons in DSF-, SPC-, and SPI-based particleboards, water, and solid water phantoms with incident photon energies ranging from 1 keV to 65 MeV obtained with the Monte Carlo EGSnrc PEGS4 calculations, are also presented.

Chapter 5 summarizes the overall findings obtained from this thesis and provides further recommendations for future research in the construction of bio-based tissue substitute phantoms made from *R. spp*. particleboards.

CHAPTER 2

LITERATURE REVIEW

2.1 Radiation Therapy (RT) Overview

Radiation therapy (RT) is an important part of conventional systematic cancer treatment and prevention of the spread of malignant diseases. Effectiveness of treatment has been shown to contribute to the cure of different forms of cancer. One of the major improvements of RT is to increase the treatment dose to the tumor. The main limiting factor for greater dosage delivery to tumor cells however, are normal tissue tolerances (Suit, 2002). RT can be administered using heavy charged particles, gamma irradiation emitted from ^{60}Co, and high energy photons and electrons irradiation produced with a LINAC. The utilization of cobalt teletherapy has reduced and is almost no longer used by the 1990s because of the associated deficiency such as the difficulty to control the equipment and the lifespan of the ^{60}Co source that has a half-life of approximately five years. Modern treatment techniques in clinical EBRT are raising growing demands on the accuracy and speed of algorithms for computing the dose. Much interest has been generated in conformal treatment planning during the last decade, such as IMRT, volumetric modulated arc therapy (VMAT), image-guided radiation therapy (IGRT), SRS, and SBRT (Negm et al., 2020).

Electron beams have been used successfully in numerous sites such as the head and neck to avoid irradiation of the spinal cord. It is also used for RT to the chest wall to prevent excessive lung irradiation (Negm et al., 2020). The dynamic existence of interactions between electrons and tissue means that typically, electron beams are difficult to model. Especially challenging in electron beam therapy are the measurement of collimator scatter and leakage, dose estimation in small fields, circumstances involving abrupt shifts in surface contours, slight inhomogeneities, and oblique beam

incidences (O'Shea, 2011). The typical EBRT pathway is patient immobilization and imaging with modalities ranging from CT, MRI, PET, ultrasound or basic X-ray radiography, tumor segmentation, margins considering essential structures prior to image validation procedures, and TPS (Tino et al., 2020).

LINACs were clinically available as early as the 1950s but widespread use came about in the 1970s. A typical clinical LINAC has photon beam ranges from 6 MV to 18 MV as well as nominal electron beams between 6 MeV to 20 MeV. While the photon beam can penetrate the deeper field, the electron beam provides more distinct advantages in terms of the uniformity of the radiation towards the target and minimizing the dose to deeper tissues (Khan, 2010).

2.2 Description of LINAC and its Component Systems

There are many advanced tools in use for the treatment of cancer but the LINAC remains the most commonly used source of radiation. Deep-seated tumors are typically treated with X-rays formed by bremsstrahlung from interaction of an electron beam with a target. However, superficial tumors are usually treated using the electron mode of a LINAC (Vega-Carrillo et al., 2010). Figure 2.1 displays the key components of an Elekta Synergy PRIMUS LINAC for clinical use with addition of particleboard phantom samples. The LINAC customizes high energy X-rays or electrons to conform to a tumor shape and destroy cancer cells by causing irreparable damage to their DNA while preventing possible harm to normal tissue (Mittal et al., 2011).

Figure 2.1: Elekta Synergy PRIMUS LINAC (Advanced Medical and Dental Institute, Universiti Sains Malaysia, USM) and particleboard phantom samples.

A LINAC generator is called a klystron. The klystron provides the electrons with the radiofrequency (RF) wave. The electron gun and microwave source are pulsed to inject the high velocity electrons into the accelerating waveguide at the same time as the microwaves energize them. The accelerating electrons tend to diverge, partly because of mutual Coulomb repulsion but mainly because there is a radial component in the electric fields in the waveguide structure. However, by using a coaxial magnetic focusing field, this divergence can be reduced, and the electrons are directed back on their straight path. There are also additional steering coils which can be used to guide the electron beam so that it emerges from the appropriate position and direction from the accelerator structure (Greene and Williams, 1997). Figure 2.2 provides a schematic diagram of the various sections of a LINAC necessary for radiation beam generation.

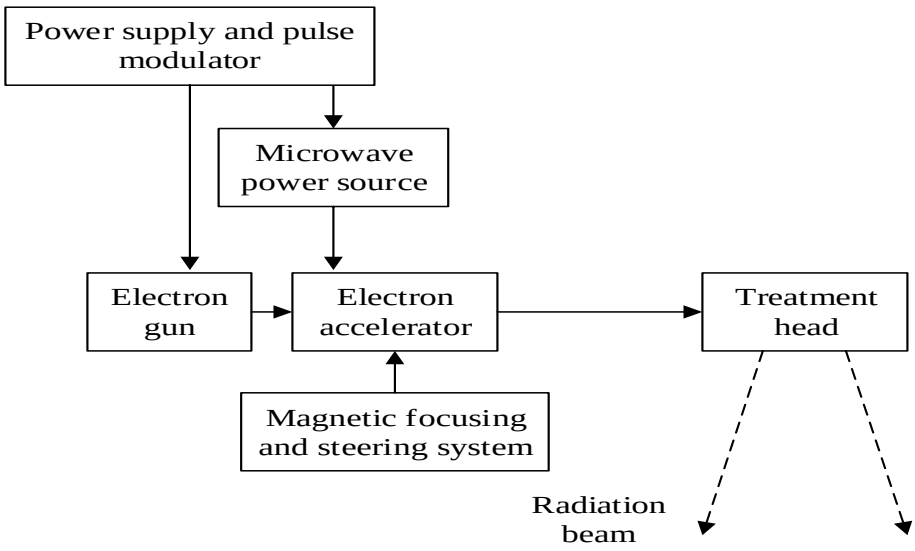

Figure 2.2: Schematic diagram of the various sections of a LINAC for radiation beam generation.

The LINAC's main mechanical elements are the gantry and patient systems, which serve to orientate the radiation source in relation to the patient lying on the patient support and positioning system. The radiation beam that emerges from the multileaf collimator (MLC) is often directed through the gantry axis and oriented around it. The couch incorporates three linear motions and a rotation motion about the isocenter to support the patient positioning for treatment. The accelerating electrons will enter the treatment head and pass through a bending magnet, where the electrons are either bent at 90^{o} or 270^{o}. The 90^{o} bending system will create a larger focal spot around the electron beam with slightly different electron energies, while the 270^{o} will create a smaller focal spot with almost identical electron energies.

The treatment head includes a beam monitor consisting of detectors which are used both to determine the transmitted dose and to provide the accelerator and its related systems with control signals for the safety interlock and feedback systems. When the electron beam is to be used for treatment, to provide the necessary field coverage, it is removed from the vacuum system through a thin window into the treatment head where

it is dispersed. The final beam collimation is done with an electron beam applicator which mounts on the treatment head externally as well. The applicator is made of low atomic number metal such as aluminum with varying field sizes from 5×5 cm^2 to 25×25 cm^2. During treatment, the applicator is brought close to the surface of the patient or phantom to reduce the dose beyond the collimated beam that is leading to the distribution of the electrons.

Photons are formed when the high speed electrons in the treatment head bombard the target material. The target materials are usually materials with high atomic numbers such as gold to generate photons with high energy. With the help of a flattening filter the photons emitted from the target are filtered. Two sets of collimator which make up the jaws give a rectangular shape to the X-ray beams coming out of the treatment head. Additionally, a light indicator that simulates the shape of the collimated X-ray beams indicates the size of the photon beams (Loverock, 2007).

2.3 Comparison of Dosimeters in RT

Dosimeters used in RT are primarily concerned with assessing the absorbed dose from a radiation source which delivers either photons or electrons. Dosimeters are classified into two types, that is, absolute and relative dosimeters. The absolute dosimeter generates a signal from which the dose in its sensitive volume can be calculated without requiring calibration in a known radiation field, while relative dosimeter involves calibration of its signal in a known radiation field. The dosimeters used in RT currently include air and liquid-filled ICs, films, thermoluminescent dosimeters (TLDs), metal-oxide semiconducting field-effect transistors (MOSFETs), silicon diodes, optically-stimulated luminescence (OSL) dosimeters, and fiber-optic-coupled dosimeters (Knoll, 2000; Dreindl et al., 2014). Desirable dosimeters can be

characterized with some specific properties such as accuracy and precision, dose rate dependence, energy response, directional dependence, spatial resolution, and stability (Jordan, 2009). In this study, cylindrical Farmer-type ICs and Gafchromic EBT3 films which are discussed in detail in the following section are used because of their advantages that make them attractive tissue-equivalent dosimeters for RTD.

2.3.1 Ionization Chamber (IC) Dosimeters

The most commonly used types of dosimeters in RT for accuracy and dependability are the ICs (Jordan, 2009). This is because of their specific characteristics such as high-precision, stability, excellent linearity, uniform energy response, little to no fading and dose rate dependence due to general ion recombination. They serve as absolute radiation dosimeters in the calculation of absorbed dose for high energy photon and electron beams such as the cylindrical Farmer-type chamber and plane parallel-type ICs.

Standard dosimetry protocols are based on the Bragg–Gray cavity theories that provide a simple linear relationship between the absorbed dose in a dosimeter and the absorbed dose in the cavity medium containing the dosimeter (Knoll, 2000). As demonstrated in Figure 2.3, the energy lost E in collision interaction by a fluence of Φ (C/cm^2) of energy T_0 passing perpendicularly through a foil of mass thickness ρt (g/cm^2) can be expressed as follows (Equation 2.1) (Knoll, 2000):

$$E = \Phi \left(\frac{dT}{\rho dx}\right)_t \rho t \tag{2.1}$$

where, $\left(\frac{dT}{\rho dx}\right)_t$ denote the mass collision stopping power of the foil medium. The absorbed dose in the foil can be expressed in terms of the cavity (c) between the two media, as given below (Equation 2.2 and Equation 2.3) (Knoll, 2000):

$$D_g = \Phi \left[\left(\frac{dT}{\rho dx} \right)_{c,g} \right]_T \tag{2.2}$$

$$D_w = \Phi \left[\left(\frac{dT}{\rho dx} \right)_{c,w} \right]_T \tag{2.3}$$

where, D_g and D_w are the respective absorbed dose in the cavity medium g and w. By ignoring backscatter and applying the Bragg–Gray conditions, for a differential energy distribution Φ_T, the appropriate average mass collision stopping power is given by Equation 2.4 and Equation 2.5 (Knoll, 2000):

$${}_{\mathrm{m}}\bar{S}_g \equiv \frac{\int_0^{T_{max}} \Phi_T \left(\frac{dT}{\rho dx} \right)_{c,g} dT}{\int_0^{T_{max}} \Phi_T dT} = \frac{1}{\Phi} \int_0^{T_{max}} \Phi_T \left(\frac{dT}{\rho dx} \right)_{c,g} dT = \frac{D_g}{\Phi} \tag{2.4}$$

$${}_{\mathrm{m}}\bar{S}_w \equiv \frac{\int_0^{T_{max}} \Phi_T \left(\frac{dT}{\rho dx} \right)_{c,w} dT}{\int_0^{T_{max}} \Phi_T dT} = \frac{1}{\Phi} \int_0^{T_{max}} \Phi_T \left(\frac{dT}{\rho dx} \right)_{c,w} dT = \frac{D_w}{\Phi} \tag{2.5}$$

Combining the above equations, yields Equation 2.6:

$$\frac{D_w}{D_g} = \frac{{}_{\mathrm{m}}\bar{S}_w}{{}_{\mathrm{m}}\bar{S}_g} \equiv {}_{\mathrm{m}}\bar{S}_g^w \tag{2.6}$$

where, ${}_{\mathrm{m}}\bar{S}_g$ and ${}_{\mathrm{m}}\bar{S}_w$ are the respective stopping power in the cavity medium g and w. Assuming the medium occupying the cavity to be a gas in which a charge Q is produced by the radiation, the absorbed dose in cavity medium g (D_g) can be expressed as given in Equation 2.7 (Knoll, 2000):

$$D_g = \frac{Q}{m} \left(\frac{\bar{W}}{e} \right)_g \tag{2.7}$$

where, $\bar{W}$ is the mean energy spent, e is the electron charge, m is the sensitive air mass, and $\left(\frac{\bar{W}}{e} \right)_g$ denotes the mean energy spent per unit charge produced (JC^{-1}). Putting

Equation 2.7 into Equation 2.6, the Bragg–Gray relation was obtained in terms of cavity ionization (Equation 2.8) (Knoll, 2000):

$$D_w = \frac{Q}{m}\left(\frac{\overline{W}}{e}\right)_g \cdot {}_{\mathrm{m}}\bar{S}_g^w \tag{2.8}$$

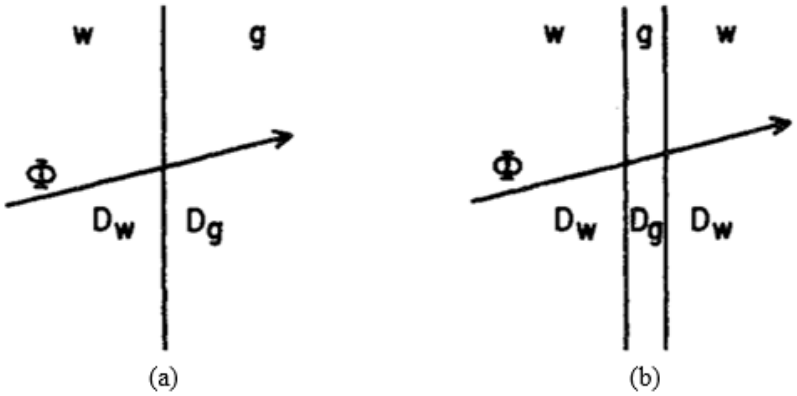

Figure 2.3: Bragg–Gray cavity (c) theories between the absorbed dose in a dosimeter for two medium (w and g) (Knoll, 2000).

2.3.2 Film Dosimeters

The two kinds of film used for dosimetry purposes are silver halide radiographic and radiochromic films. Radiographic film dosimeters are integrative, have no angular dependence, and have the ability to provide excellent measurements of dose distribution due to their extremely high spatial resolution. They however, suffer from energy dependence and non-tissue equivalence. On the other hand, radiochromic film exhibits tissue equivalence, and can give excellent spatial resolution that does not require a special developmental procedure and provides permanent absolute absorbed dose values with reasonable precision and consistency (Seco et al., 2014).

A common radiochromic film for RTD applications is Gafchromic EBT (Gafchromic Extended Beam Therapy) film. Gafchromic EBT film improved on existing radiographic films as it had a similar atomic number and composition as that of tissue and featured a self-developing polymerization based process. Some of the

shortcomings of EBT film are film non-homogeneity, post-exposure growth, sensitivity to polarization, non-reusable, and environmental dependencies like temperature and humidity (Dreindl et al., 2014). The next generation of EBT film was Gafchromic EBT2. Unlike EBT, EBT2 film had one asymmetric active layer and additional adhesive layer. However, this asymmetric layer introduced a facing up/down scan orientation dependence. EBT2 also introduced a yellow-dyed synthetic polymer as the active layer of the film, with the goal of increasing film uniformity (Richley et al., 2010).

A new radiochromic film, model EBT3, have been investigated with characteristics, such as response at high-dose levels, sensitivity to scanner orientation and post-irradiation coloration, energy and dose rate dependence, and orientation dependence with respect to the film side. In addition, a matte polyester layer has been added to the EBT3 film to prevent the formation of Newton's rings during scanning, which were commonly observed when using EBT2 films (Seco et al., 2014). The characteristics of radiochromic films are highlighted in Figure 2.4.

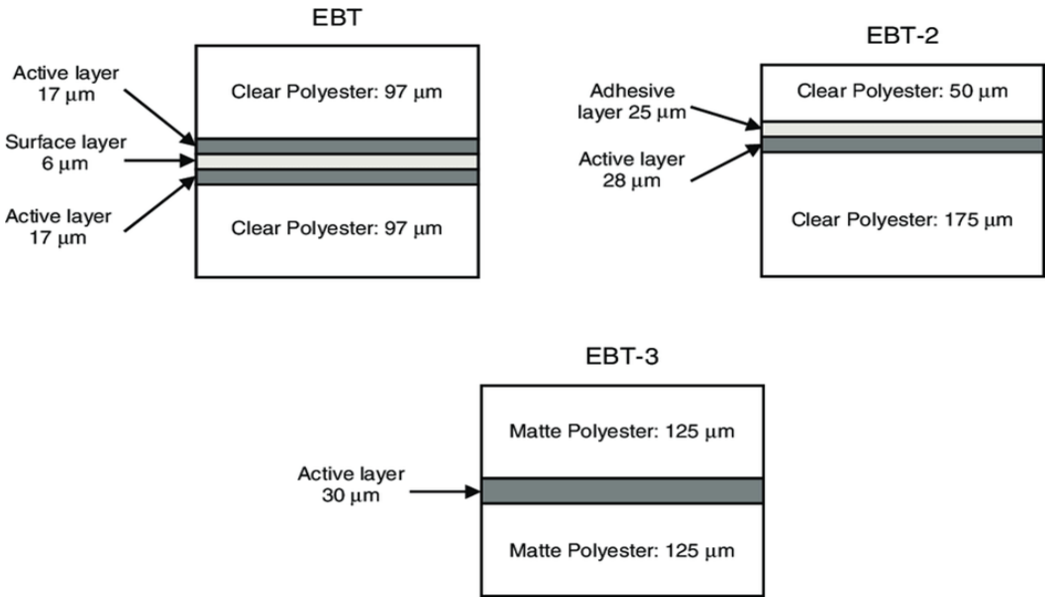

Figure 2.4: Schematic cross-sectional structure of radiochromic films (Seco et al., 2014).

2.4 Monte Carlo Simulation Using EGSnrc PEGS4 for Probability of Photon Interactions

Monte Carlo (MC) simulation is a precise and accurate method of modelling the complex configurations of the photon and electron interactions in RT. The MC technique can be characterized as a statistical device, using random numbers to simulate and replicate events that can be interpreted via stochastic processes. Unlike traditional techniques of discrimination, statistical simulations in the physical process need not be described by mathematical equations to be solved, simply because this process can be defined by a probability density function, which characterizes the observed phenomenon. MC can unravel a significant number of electron transport problems with conventional treatment planning algorithms, especially with in-patient heterogeneities (Negm et al., 2020).

MC models of radiation treatment machine heads provide realistic means of obtaining energy spectra and angular distributions of photons and electrons (Figure 2.5). To confirm the validity of the energy spectra and angular distributions produced by the MC programs, the probability of photon interactions can be calculated and the results obtained can be compared with those of appropriate standard phantoms. There are several factors that may affect the final model, such as the selected MC dose engines including: EGS, GEANT, MCNP, and PENELOPE, which can be distinguished by their particle of interest and cross-section data. Due to user-friendly functionality, the MC simulations in this work were carried out mainly using the EGSnrc PEGS4 (EGSnrc – electron gamma shower by National Research Council of Canada, Ottawa, Canada, PEGS4 – pre-electron gamma shower 4) program, and coupled with the fact that it has modification options (Júnior et al., 2015; Kawrakow et al., 2013).